

# Energy and polarization based on-line interference mitigation in radio interferometry

Sarod Yatawatta, Albert-Jan Boonstra, Chris P. Broekema

<sup>a</sup>*ASTRON, The Netherlands Institute for Radio Astronomy, Oude hoogeveensedijk, Dwingeloo, The Netherlands*

---

## Abstract

Radio frequency interference (RFI) is a persistent contaminant in terrestrial radio astronomy. While new radio interferometers are becoming operational, novel sources of RFI are also emerging. In order to strengthen the mitigation of RFI in modern radio interferometers, we propose an on-line RFI mitigation scheme that can be run in the correlator of such interferometers. We combine statistics based on the energy as well as the polarization alignment of the correlated signal to develop an on-line RFI mitigation scheme that can be applied to a data stream produced by the correlator in real-time, especially targeted at low duty-cycle or transient RFI detection. In order to improve the computational efficiency, we explore the use of both single precision and half precision floating point operations in implementing the RFI mitigation algorithm. This ideally suits its deployment in accelerator computing devices such as graphics processing units (GPUs) as used by the LOFAR correlator. We provide results based on real data to demonstrate the efficacy of the proposed method.

*Keywords:*

Radio astronomy, RFI, Reinforcement learning, Finite precision arithmetic

---

## 1. Introduction

Various human-made electromagnetic signals are received by radio telescopes and act as unwanted interference. Mitigation of such RFI has been extensively researched and many algorithms exist for this purpose, (e.g. Leshem et al., 2000; Leshem and van der Veen, 2000; Fridman and Baan, 2001; Raza et al., 2002; Bentum et al., 2008; Hellbourg et al., 2012; Oftringa et al., 2010; Baan, 2019; Cucho-Padin et al., 2019; Vos et al., 2019). However, new sources of RFI are still emerging, (e.g. Brentjens, 2016; Winkel and Jessner, 2019; Sokolowski et al., 2016; Vruno et al., 2023; Bassa et al., 2024) that require continuous investment on better RFI mitigation algorithm development.

The majority of existing RFI mitigation algorithms are off-line, i.e., they operate on data that are stored on disk. On the other hand, on-line RFI mitigation algorithms (Van Nieuwpoort, 2016; Van Nieuwpoort et al., 2018; Smith, 2022; Rafiei-Ravandi and Smith, 2023; Sclocco et al., 2020) operate on data streams in real-time. There are several differences between the off-line and the on-line RFI mitigation algorithms. Off-line algorithms have access to the full time-frequency domain (or footprint) of the data and

can access the data multiple times. This is because the data are channelized in frequency and averaged over time to reduce the raw data volume as much as possible before storing on disk. Hence, sophisticated algorithms can be developed for off-line RFI mitigation, provided the data storage and computational costs are not a limitation. In contrast, on-line algorithms can only access the data once to determine the presence or absence of RFI, and the time-frequency domain of the data being accessed at any given instance is small. A key characteristic of an on-line RFI mitigation algorithm is its computational efficiency, making the run-time of such an algorithm to be lower than the duration of the data being considered (real-time). A distinct advantage of a real-time and on-line RFI mitigation algorithm is its applicability to data streams at a high time-frequency resolution. For example, in the LOFAR correlator (Broekema et al., 2018), one second of post-correlation data is produced by averaging thousands of samples taken at a much higher time resolution. In such a situation, RFI that have a small duty cycle (having a duration of much less than one second) that are also called as 'transient' (Gehlot et al., 2024) or 'short duration' (Cucho-Padin et al., 2019) RFI will be averaged with RFI free data,

thus diluting the contribution of the RFI over the full one second period. In fact, such averaged and diluted RFI can pass through undetected by conventional off-line RFI mitigation methods and can appear as weak RFI at later stages of data processing (lowering the scientific quality of the data). Therefore, an on-line RFI mitigation algorithm applied before the averaging of the data can mitigate such RFI signals and improve the quality of the averaged data.

In this paper, we propose a post-correlation RFI mitigation algorithm that can operate on-line and in real-time. We consider data streams that have full polarization and we use both the energy (spectral kurtosis, e.g., Nita and Gary, 2010; Nita and Hellbourg, 2020; Smith et al., 2022) as well as the polarization alignment (directional statistics, e.g., Guo et al., 2013, 2015; Yatawatta, 2021) of the data stream to detect and mitigate RFI. In order to improve the computational efficiency of the proposed algorithm, we exploit the use of mixed precision floating point operations, making the proposed algorithm ideally suited to be used in the LOFAR correlator (Broekema et al., 2018) that will (in the future) have hardware (graphics processing units GPUs) for reduced precision computing (Ho and Wong, 2017). The optimization of computational routines (kernels) for other tasks such as image synthesis (Corda et al., 2022) using generic tools such as the kernel tuner (van Werkhoven, 2019) already exist. In this paper however, we consider optimization at a lower level (running down to each instruction) and the parameter space has a much higher dimensionality. Hence, we use reinforcement learning (RL Sutton and Barto, 2018; Yatawatta, 2024) to perform this optimization.

The contributions of this paper can be summarized as follows:

- We propose an RFI mitigation algorithm that uses both the energy (spectral kurtosis) as well as the polarization alignment (directional statistics) of the data, while most existing algorithms only use the energy of the data for detection of RFI (note that spectral kurtosis is a higher order statistic based on the energy of the data while most methods use second order statistics). Therefore, as shown in Yatawatta (2021), we are able to detect RFI that have lower energy than what can be detected by conventional methods when the same time-frequency domain of the data is being used for the RFI detection.

- The proposed RFI mitigation algorithm can be deployed in an on-line and real-time manner, ideally suited to be used within the LOFAR correlator that uses GPUs (Broekema et al., 2018). This is particularly aimed at detecting transient or short duration RFI (Gehlot et al., 2024; Cucho-Padin et al., 2019) that may possibly be diluted with RFI free data otherwise.
- In order to improve the computational efficiency, we explore the use of reduced precision floating point operations, namely, 32 bit single precision and 16 bit half precision operations in the computational routines that detect and mitigate the RFI. The data stream itself has a fixed 32 bit precision and we do not change that but rather, the computations performed during the RFI mitigation. We only consider 16 bit or 32 bit precision in this paper because of several reasons. First, while modern GPU hardware mostly support 64 bit, 32 bit or 16 bit arithmetic (Ho and Wong, 2017; Luo et al., 2024), we leave out 64 bit precision because the input is already at 32 bit precision. Secondly, by keeping the choice between 32 or 16 bits, we keep the problem simple for the reader to understand without the loss of generality. However, the method described in this work can be applicable to, say, mixing floating point arithmetic with 64, 32, 16 or 8 bit precisions. In order to decide the best precision to use for each floating point operation, we use reinforcement learning. The novel use of RL for tuning of hybrid precision computation is demonstrated using RFI mitigation as an application but it can also be used in many other applications in the future.

The rest of the paper is organized as follows: in section 2, we provide an overview of the on-line RFI mitigation strategy using both energy and polarization. Next, in section 3, we provide the optimization of the core computing steps (CUDA kernel) to use mixed precision floating point arithmetic. In section 4, we provide results based on simulations and real data to illustrate the efficacy of the proposed method. Finally, we draw our conclusions in section 5.

Notation: The sets of real and complex numbers are denoted by  $\mathbb{R}$  and  $\mathbb{C}$ , respectively.

## 2. Energy and polarization based RFI mitigation

We consider the output of a correlator that is fed by dual (linear) polarized data streams from each station or receiver. The instantaneous output of the correlator for a given pair of receivers (a baseline) can be given as

$$\mathbf{V}_i = \begin{bmatrix} xx_i & xy_i \\ yx_i & yy_i \end{bmatrix} \quad (1)$$

where we use the subscript  $i$  to denote the time-frequency sampling point for the given receiver pair and  $xx_i, xy_i, yx_i, yy_i \in \mathbb{C}$  are the correlations produced by the correlator. Given  $N$  receivers, the correlator will produce  $N(N+1)/2$  data streams at the output and we perform RFI mitigation on each of them separately. Normally, the instantaneous output (1) is averaged over  $i$  using thousands of samples before the averaged data is sent to storage on disk.

Assuming linear polarized feeds, we can form the complex Stokes parameters for (1) as

$$\begin{aligned} \mathcal{I}_i &\triangleq xx_i + yy_i, \\ \mathcal{Q}_i &\triangleq xx_i - yy_i, \\ \mathcal{U}_i &\triangleq xy_i + yx_i, \\ \mathcal{V}_i &\triangleq j(xy_i - yx_i) \end{aligned} \quad (2)$$

where  $\mathcal{I}_i, \mathcal{Q}_i, \mathcal{U}_i, \mathcal{V}_i \in \mathbb{C}$ . We consider a window with indices in the set  $\mathcal{W}$  with  $W$  elements for detection of RFI. In off-line RFI mitigation methods,  $W$  can be arbitrarily large but in our case,  $W$  is small, typically a handful of data samples.

### 2.1. Flagging using spectral kurtosis

Post correlation spectral kurtosis statistics (Nita and Hellbourg, 2020) can be extracted using the data window as

$$S_1 = \sum_{i \in \mathcal{W}} |\mathcal{I}_i| \quad S_2 = \sum_{i \in \mathcal{W}} |\mathcal{I}_i|^2. \quad (3)$$

The statistic for determining the presence or absence of RFI is given as (Nita and Gary, 2010)

$$\tau_{\text{SK}} = \frac{W}{W-1} \frac{d+1}{S_1^2} \left( \frac{W S_2}{S_1^2} - 1 \right) \quad (4)$$

where  $d$  is given a priori based on the distribution of RFI free data (typically  $d \in [0.5, 1]$ ) but can be fine tuned as in Nita and Hellbourg (2020)). The spectral

kurtosis based statistic above is compared to lower and upper limits that are pre-determined,

$$\text{flag} = \tau_{\text{SK}} < s_{\text{low}} \quad \text{OR} \quad \tau_{\text{SK}} > s_{\text{high}} \quad (5)$$

and if data within the window  $\mathcal{W}$  are flagged, they are excluded from the summation to produce the output (and the weight of the data is also updated).

### 2.2. Flagging using directional statistics of polarization

In order to extract the directional statistics (Guo et al., 2013; Yatawatta, 2021), we work on both the real and imaginary parts of  $\mathcal{Q}_i, \mathcal{U}_i$ , and  $\mathcal{V}_i$  separately. Without loss of generality, let  $q_i, u_i$ , and  $v_i$  ( $\in \mathbb{R}$ ) be the real or imaginary parts of  $\mathcal{Q}_i, \mathcal{U}_i$ , and  $\mathcal{V}_i$  respectively.

For each data point  $i$  ( $\in \mathcal{W}$ ) we construct the polarization vector as

$$p_i = \sqrt{q_i^2 + u_i^2 + v_i^2} \quad (6)$$

and thereafter, the normalized polarization components are calculated as

$$\hat{q}_i = q_i/p_i, \quad \hat{u}_i = u_i/p_i, \quad \hat{v}_i = v_i/p_i. \quad (7)$$

The average polarization within the window  $\mathcal{W}$  is calculated as

$$q = \sum_{i \in \mathcal{W}} \hat{q}_i, \quad u = \sum_{i \in \mathcal{W}} \hat{u}_i, \quad v = \sum_{i \in \mathcal{W}} \hat{v}_i \quad (8)$$

and the directional statistic as

$$r = \sqrt{q^2 + u^2 + v^2}/W. \quad (9)$$

With RFI, the directional statistic will be more prominent and therefore can be compared to a pre-defined threshold  $\gamma$  to determine whether to flag the data within the window  $\mathcal{W}$  or not, i.e.,

$$\text{flag} = r > \gamma. \quad (10)$$

The flags derived from the real parts and imaginary parts of  $\mathcal{Q}_i, \mathcal{U}_i$ , and  $\mathcal{V}_i$  are combined using the logical OR operation before applying to the data. Finally, the flags derived from spectral kurtosis in section 2.1 and directional statistics in section 2.2 are combined using the logical OR operation for applying them to the data.

Note that the hyperparameters and thresholds  $d, s_{\text{low}}, s_{\text{high}}$  and  $\gamma$  used above are kept constant in the

above description but there are (mostly theoretical) ways of tuning these parameters for optimal performance (e.g. Nita and Gary, 2010; Yatawatta, 2021) but we leave out this aspect for future work. Since the RFI mitigation is performed on per-baseline basis, the calibration of such data should ideally consider the weights attributed to each data point, for instance by using robust techniques (Kazemi and Yatawatta, 2013).

### 3. Mixed precision optimization using reinforcement learning

In this section, we break down the algorithms described in sections 2.1 and 2.2 into a set of instructions that can be performed in an arbitrary precision format. The optimal precision to use is determined by satisfying two criteria:

- Accuracy: The end result of the algorithm should agree with the end result obtained by the same algorithm using double precision (64 bit) floating point operations. We consider the double precision floating point result as the ground truth. Note however that the end result of the overall algorithm is a flag (a one or a zero), i.e., a value with 1 bit precision. Therefore, theoretically there should be a way to reduce the precision from the starting precision of 32 bits to one bit and the objective of this optimization is to find this optimal way. However, we remind the reader that the data stream that is being processed is kept fixed at 32 bit precision.
- Cost: The overall computational cost should be as low as possible. Let  $C$  be the cost of an operation in any floating point precision. We use  $C = 1$  for one single precision (32 bit) operation and (arbitrarily) set  $C = 0.6$  for one half precision (16 bit) operation. More exact costs for these operations can be used for optimizing the algorithms for any specific GPU. Obviously, we do not use double precision for calculation of the cost because it will not be used in the practical algorithm (only used for ground truth calculation).

The input  $\mathcal{I}_i$ ,  $\mathcal{Q}_i$ ,  $\mathcal{U}_i$ , and  $\mathcal{V}_i$  are single precision (32 bit) floating point data. In Table 1, we have broken down the spectral kurtosis based RFI mitigation algorithm described in section 2.1 into groups of operations. For each group listed in Table 1, we use the

same precision floating point format. For example, for group 2 in Table 1, we can either use half precision or single precision, and the cost for this group should be  $W \times 0.6$  for half precision or  $W \times 1$  for single precision, respectively.

Table 1: Operations for spectral kurtosis based flagging for window size of  $W$  data points. The cost given on the right hand column should be multiplied by  $C$  for the precision chosen for each group. The constants  $d$ ,  $s_{low}$ ,  $s_{high}$  are given as well as  $\epsilon$  which is kept at a possibly low and positive value depending on the precision. The real and imaginary parts of  $\mathcal{I}_i$  are given by  $xr_i$  and  $xi_i$ , respectively.

Group	Operation	Cost
1	$x2_i \leftarrow xr_i^2 + xi_i^2 \quad \forall i$	$3W$
2	$xa_i \leftarrow \sqrt{x2_i} \quad \forall i$	$W$
3	$S_1 \leftarrow \sum_i xa_i$	$W$
4	$S_2 \leftarrow \sum_i x2_i$	$W$
5	$\tau \leftarrow \frac{Wd+1}{W-1}$	1
6	$S_{12} \leftarrow S_1^2$	1
7	$\tau \leftarrow \tau \frac{WS_2}{S_{12}+\epsilon} - 1$	1
7	$\tau < s_{low}$ OR $\tau > s_{high}$	2

In the same manner, we have expanded the RFI mitigation algorithm based on the directional statistics of polarization (section 2.2) in Table 2.

Table 2: Operations for directional statistics of polarization based flagging for window size of  $W$  data points. The inputs  $q_i, u_i$  and  $v_i$  are either the real or the imaginary parts of  $\mathcal{Q}_i$ ,  $\mathcal{U}_i$ , and  $\mathcal{V}_i$ . The cost given on the right hand column should be multiplied by  $C$  for the precision chosen for each group. The constant  $\gamma$  is given a priori as well as  $\epsilon$  which is kept at a possibly low and positive value depending on the precision.

Group	Operation	Cost
1	$q2_i, u2_i, v2_i \leftarrow q_i^2, u_i^2, v_i^2 \quad \forall i$	$3W$
2	$p_i \leftarrow \sqrt{q2_i + u2_i + v2_i} + \epsilon \quad \forall i$	$3W$
3	$\hat{q}_i, \hat{u}_i, \hat{v}_i \leftarrow q_i/p_i, u_i/p_i, v_i/p_i \quad \forall i$	$3W$
4	$q, u, v \leftarrow \sum_i \hat{q}_i, \hat{u}_i, \hat{v}_i$	$3W$
5	$q2, u2, v2 \leftarrow q^2, u^2, v^2$	3
6	$r \leftarrow \sqrt{q2 + u2 + v2}/W$	4
7	$r > \gamma$	1

Looking at Tables 1 and 2, we have 14 groups of operations. If we have the choice of selecting either single precision or half precision for each of these operations, we have  $2^{14}$  possible choices to consider. The reasons for using reinforcement learning (Sutton

and Barto, 2018; Yatawatta, 2024) for making the optimal selection of precision for each group of operations can be elaborated as follows.

- The curse of dimensionality: Having to consider  $2^{14}$  choices by exhaustive search could be feasible with modern compute capabilities, but we foresee the option of having more choices for the precision of each group of operations, for instance by adding 8 bit precision. In such a situation, exhaustive search of  $3^{14}$  options is clearly not computationally efficient.
- We are not interested in finding the optimal precision configuration to use for any one given data realization. In contrast, we need to find a configuration that performs well over all data. Statistically speaking, we need the solution to be marginalized over the data distribution and in order to perform that, having a model to predict the configuration to use given any data realization is needed. By training an RL agent, we are able to create this model.

We only provide the essential details of the formulation of the optimization as an RL problem, and further details can be found in for example, (Yatawatta, 2024). The RL agent interacts with the problem (also called the environment) in order to learn and find the optimal solution. We use the soft-actor-critic (SAC Haarnoja et al., 2018a,b) algorithm for training our RL agent. The three concepts that need clear definition in any RL application are the state, the action and the reward, and we elaborate on this in the following text.

### 3.1. The action

The optimal precision to use for any given situation is produced by the agent as the action  $a \in [0, 1]^{14}$ . The 14 values in the action correspond to the number of groups of operations in Tables 1 and 2. If  $a[i] < 0.5$  the  $i$ -th group precision is set to 32 bits (single precision) else it is set to 16 bits (half precision).

### 3.2. The state

The state consists of information about the data, the current precision being used and the floating point error as compared to the ground truth. We consider a data window of size  $W$  divided into  $T$  time samples and  $F$  frequency samples, i.e.,  $W = T \times F$ . Each data

point has 4 complex values and 8 real values (in 32 bit precision). The statistics of the data are extracted as  $\log \sum_i \text{real}(\mathcal{I}_i)^2$ ,  $\log \sum_i \text{real}(\mathcal{I}_i)^4$ ,  $\log \sum_i \text{real}(\mathcal{Q}_i)^2$ ,  $\log \sum_i \text{real}(\mathcal{U}_i)^2$ , and  $\log \sum_i \text{real}(\mathcal{V}_i)^2$  and normalized by dividing by  $W$ . The same is done for the imaginary part of each value. Therefore the data is characterized by 10 real values. Next, the current configuration of the precision being used is represented by 14 values that are either 0 or 1 (this is in fact the previous action  $a$  rounded to 0 or 1). In order to calculate the error of using reduced precision, the ground truth values of each floating point operation (7 values each for Table 1 and Table 2) are calculated using double precision (64 bit) floating point operations. Considering the fact that Table 2 is applied to the real and imaginary parts of the data separately, we have, all together  $7 + 7 + 7 = 21$  values to quantify the error. Thus, taken all into account, we have 45 values to represent the state  $s \in \mathbb{R}^{45}$ .

### 3.3. The reward and the penalty

The reward is calculated by comparing the ground truth flags (obtained by using double precision computation) to the flags obtained with the reduced precision versions of Table 1 and Table 2). For a correct match or flags, a reward of 33 for each routines in Table 1 and Table 2) are added. In order to calculate the computational cost, we set 1 for one 32 bit (single precision) floating point operation and 0.6 for one 16 bit (half precision) floating point operation. Furthermore, a unit cost 0.3 for type conversion, for example from 32 bit to 16 bit or vice versa is added whenever there is a conversion from one precision type to another precision type is required. An additional penalty of 20 for floating point overflow or underflow is added if this occurs anywhere in Tables 1 or 2. The final reward is calculated as the reward for correctness compared to the ground truth minus the cost and penalties.

With the setup described above, we train the RL agent to solve our problem, or in other words, to maximize the cumulative reward. In section 4, we present the performance of the RL agent in learning to solve the problem of finding the optimal precision configuration that maximizes the accuracy while minimizing the cost incurred.

## 4. Results

In this section we first present results in training our RL agent to solve the problem of finding the pre-

cision of each group of operations in Tables 1 and 2 to minimize the computational cost whilst preserving the accuracy. Thereafter, we provide results of RFI mitigation based on LOFAR observations that are stored on disk. The intended application of our algorithm is on-line, to data streams in the LOFAR correlator, however, in order to to a comparison with existing off-line RFI mitigation algorithms, we provide results based on data stored on disk.

#### 4.1. Reinforcement learning

We train an ensemble of  $E = 4$  RL agents to solve our problem described in section 3. We consider a time-frequency window of size  $W = 20$  data samples, that can (randomly) have various time-frequency footprints,  $T = 10, F = 2$  or  $T = 5, F = 4$ . In each episode, we generate complex, circular Gaussian data using the standard normal distribution for (1) and multiply this with a uniform-randomly selected scale factor in  $[0.01, 1000]$  as the RFI-free data. Afterwards, with a probability of 0.4, we add RFI to this data. The RFI signals are generated as follows. First, we uniform-randomly select an RFI footprint in the  $T \times F$  window. We generate the RFI signals for Stokes I, Q, U, and V by filling the RFI window with ones multiplied by a complex scale factor that is uniform-randomly selected from  $[0.01, 1000]$ . We also generate a  $2 \times 2$  matrix that is filled by complex, circular Gaussian random values with zero mean and unit variance. This is used to multiply the RFI signal window to create correlation between the polarizations of the RFI signal. Note that this simulation setup is quite general and not specialized to any specific telescope like LOFAR, but it can be done, if needed.

Using the soft actor-critic algorithm (Haarnoja et al., 2018a,b), we train the ensemble for 100000 episodes and in each episode, the RL agent can make 100 steps. Each model in the ensemble is randomly initialized and the data used for training each model is also different from one another. The reward obtained by the ensemble and the increase in the reward reaching a steady value indicating learning is shown in Fig. 1.

We use the trained ensemble to marginalize the effect of the data on the optimal action. We feed all  $E$  models in the trained ensemble with the same data for 100000 episodes and find the average action taken by each model over all episodes. The optimal action thus determined is given in Tables 3 and 4. Note that each element in the action  $a$  is in  $[0, 1]$  and

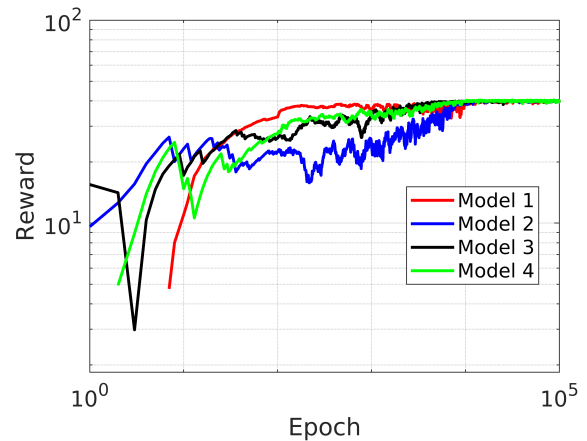


Figure 1: The reward for 100000 episodes, each episode has 100 steps. The ensemble has 4 models and each model is randomly initialized and trained using different random data.

values closer to 0 indicate single precision (32 bit) while values closer to 1 indicate half precision (16 bit) as the optimal precision to use.

Table 3: Trained operations for spectral kurtosis based flagging for window size of  $W$  data points. The hyperparameters are similar to Table 1.

Operation	Action	Precision
$x2_i \leftarrow xr_i^2 + xi_i^2 \quad \forall i$	0.000	32 bit
$xa_i \leftarrow \sqrt{x2_i} \quad \forall i$	0.000	32 bit
$S_1 \leftarrow \sum_i xa_i$	0.000	32 bit
$S_2 \leftarrow \sum_i x2_i$	0.000	32 bit
$\tau \leftarrow \frac{Wd+1}{W-1}$	0.497	16 bit
$S_{12} \leftarrow S_1^2$	0.000	32 bit
$\tau \leftarrow \tau \frac{WS_2}{S_{12}+\epsilon} - 1$	0.785	16 bit
$\tau < s_{low}$ OR $\tau > s_{high}$	0.785	16 bit

The optimal precision for each group of operations determined by the RL algorithm is also shown in Tables 3 and 4. We see that the precision changing from 32 bits to 16 bits in both algorithms which agrees with the fact that the input to both algorithms are in 32 bit precision while the output is hypothetically only 1 bit (a flag).

#### 4.2. RFI mitigation

We consider LOFAR observations taken by the low-band-antenna array (LBA) that are stored on disk. However, the proposed algorithms in Tables 3 and 4 operate with a window size  $W = 20 = 10 \times 2$

Table 4: Trained operations for directional statistics of polarization based flagging for window size of  $W$  data points. The hyperparameters are similar to Table 2

Operation	Action	Precision
$q2_i, u2_i, v2_i \leftarrow q_i^2, u_i^2, v_i^2 \quad \forall i$	0.014	32 bit
$p_i \leftarrow \sqrt{q2_i + u2_i + v2_i} + \epsilon \quad \forall i$	0.029	32 bit
$\hat{q}_i, \hat{u}_i, \hat{v}_i \leftarrow q_i/p_i, u_i/p_i, v_i/p_i \quad \forall i$	0.422	32 bit
$q, u, v \leftarrow \sum_i \hat{q}_i, \hat{u}_i, \hat{v}_i$	0.901	16 bit
$q2, u2, v2 \leftarrow q^2, u^2, v^2$	0.787	16 bit
$r \leftarrow \sqrt{q2 + u2 + v2}/W$	0.786	16 bit
$r > \gamma$	0.735	16 bit

in all examples. In contrast, the off-line RFI mitigation algorithms have access to the full time-frequency window of size  $3500 \times 64$ . In Fig. 2, we show the spectrograms for one baseline at about 14 MHz central frequency. We see that the off-line RFI mitigation algorithm flags more data than the on-line methods (correctly), mainly because of having access to the full time frequency window of size  $3500 \times 64$  and also because of the dilation of flags. In contrast, the on-line method based on energy and polarization is able to flag almost 70% of the data that are flagged by the off-line method, but only working with a much smaller window of size  $10 \times 2$ .

The results shown in Fig. 3 are also at central frequency of about 14 MHz. The major difference in this data is it is stored at a higher frequency resolution (512 channels instead of 64 channels). In Fig. 3, we compare the performance of on-line RFI mitigation with a window size  $W = 20 = 10 \times 2$  with all operations in Tables 1 and 2 in single precision and with the mixed precision as in Tables 3 and 4. The difference in the flags shown in Figs. 3 (b) and 3 (c) are almost none, quantitatively, less than 1%.

From the results in Figs. 2 and 3 we draw the following conclusions.

- The use of energy (spectral kurtosis) as opposed to polarization (directional statistics) of the data gives two independent methods for RFI mitigation as seen in the masks created by the two methods in Fig. 2 (c) and Fig. 2 (d), making the outcome of the combined method more robust.
- In certain situations, averaging of data and applying off-line RFI mitigation loses most of the

data, emphasizing the need for on-line RFI mitigation before any averaging is performed, in the correlator itself.

- The use of mixed precision operations in an optimal manner is capable of achieving the same level of performance as using high precision.

More quantitative results based on simulations (where the ground truth is available) can be found in existing work, for example (Smith et al., 2022) for spectral kurtosis based RFI mitigation and (Yatawatta, 2021) for polarization based RFI mitigation. It is also possible to use the methods proposed in the paper in an off-line manner, and in such situations, comparable or better performance can be achieved than most conventional off-line methods (Yatawatta, 2021).

## 5. Conclusions

We have proposed a novel, on-line RFI mitigation method for post-correlation interferometric data that jointly exploit the spectral kurtosis and the polarization directional statistics. We have also proposed the use of reinforcement learning for optimizing the floating point operations of the proposed algorithms to minimize the computational cost especially in GPUs. Future work on this topic will focus on implementing and deploying the proposed algorithm in the LOFAR correlator and dynamic adaptation of the threshold levels depending on the data streams. Furthermore, it is interesting to investigate if the on-line RFI detections can be used as input to on-line beamforming algorithms for spatial filtering of RFI as in Raza et al. (2002).

Source code implementing all algorithms discussed in this paper are publicly accessible at (FlagPol).

## References

- Baan, W.A., 2019. Implementing RFI Mitigation in Radio Science. *Journal of Astronomical Instrumentation* 8, 1940010.
- Bassa, C.G., Di Vruno, F., Winkel, B., Józsa, G.I.G., Brentjens, M.A., Zhang, X., 2024. Bright unintended electromagnetic radiation from second-generation Starlink satellites. *Astronomy and Astrophysics* 689, L10. 2409.11767.
- Bentum, M., Boonstra, A., Millenaar, R., Gunst, A., 2008. Implementation of LOFAR RFI mitigation strategy, in: *URSI General Assembly 2008, International Union of Radio Science, Belgium*. pp. 1–4.
- Brentjens, M.A., 2016. Interference due to wind turbines at 30-200 MHz, in: *2016 Radio Frequency Interference (RFI)*, pp. 7–10.

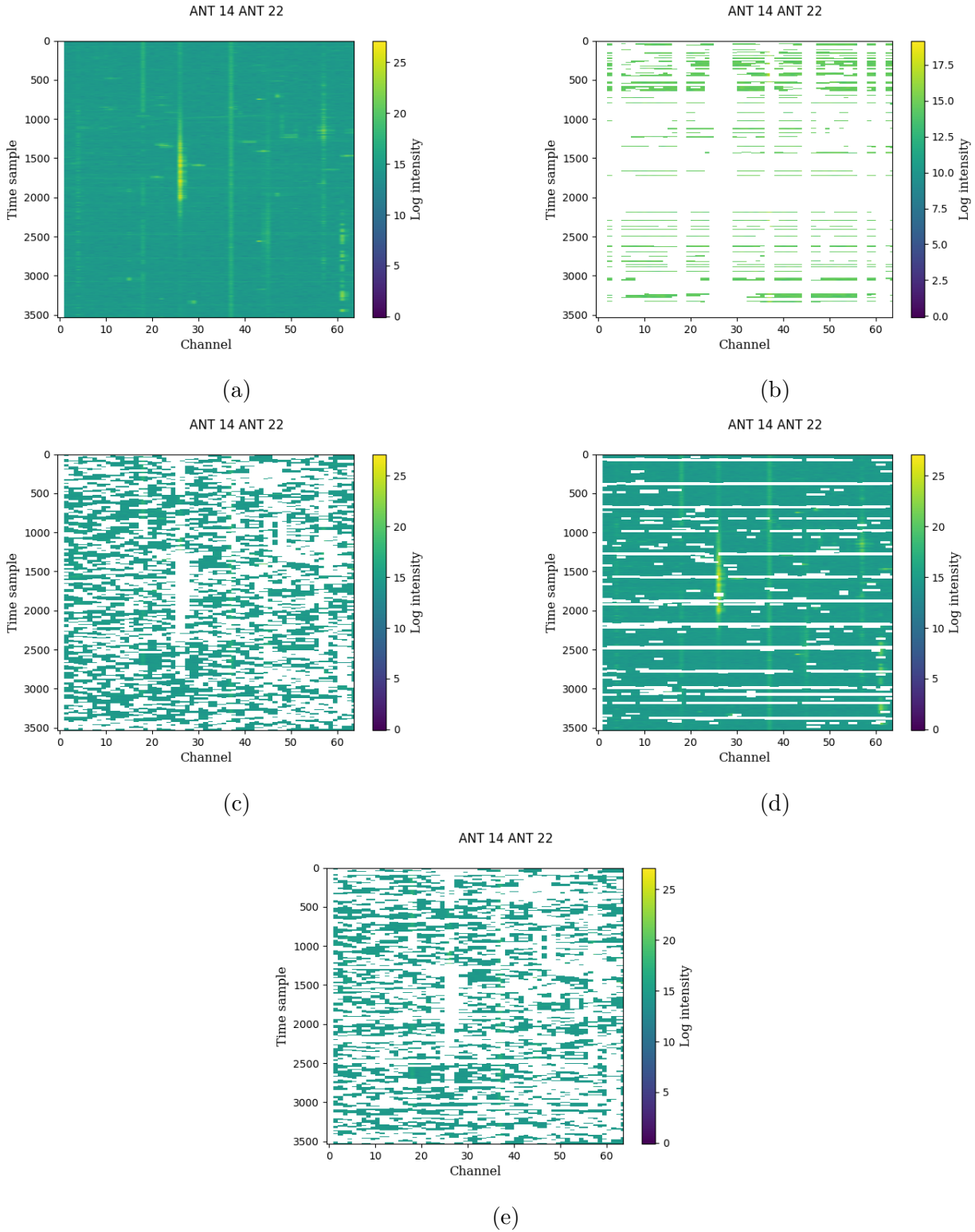
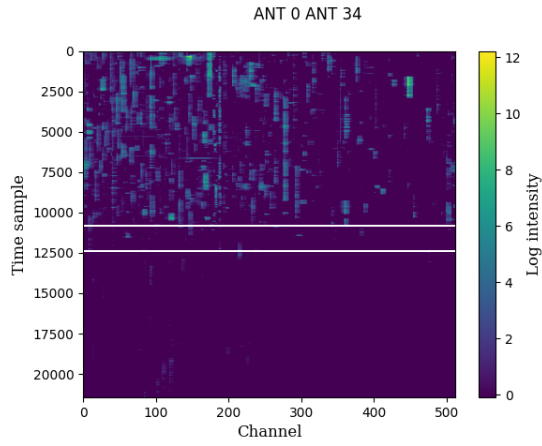
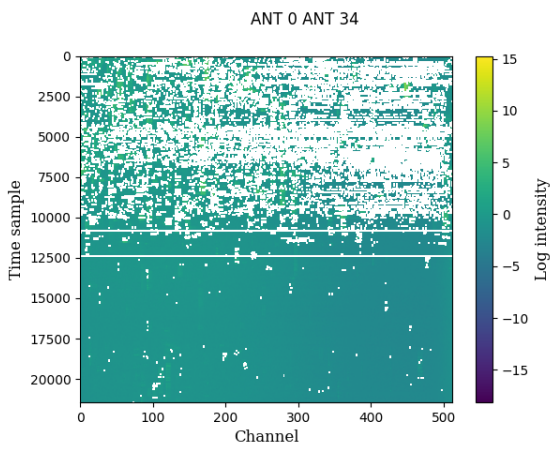


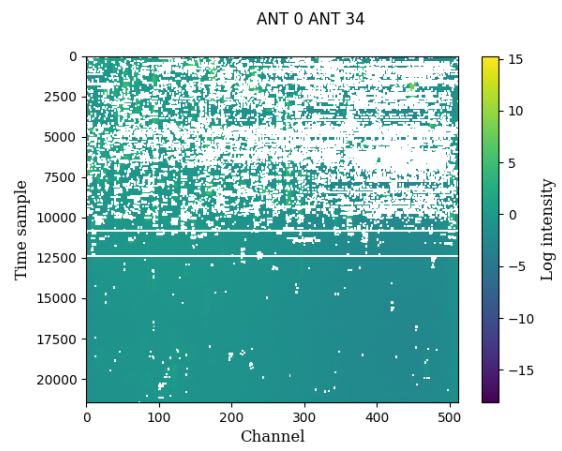
Figure 2: Waterfall plots of one baseline, Stokes I amplitude, (a) data (b) result after off-line flagging (aoflagger Offringa et al., 2010) (c) result after flagging using directional statistics of polarization as in Table 4 (d) result after flagging using spectral kurtosis as in Table 3 and (e) result after flagging using both directional statistics of polarization and spectral kurtosis. The off-line flagging uses the full time-frequency domain of size  $3500 \times 64$  while the on-line flagging only uses time-frequency windows of size  $10 \times 2$ . We see that the off-line method is able to flag more data (also by the dilation of the flag mask) than the on-line methods but the objective of the on-line method is to flag data before any averaging is being performed on the data and the above example does not represent its intended purpose.



(a)



(b)



(c)

Figure 3: Waterfall plots of one baseline, Stokes I amplitude, (a) data (b) result after on-line RFI mitigation with 32 bit operations (c) result after RFI mitigation with mixed precision operations as outlined in Tables 3 and 4.

- Broekema, P.C., Mol, J.J.D., Nijboer, R., van Amesfoort, A.S., Brentjens, M.A., Loose, G.M., Klijn, W.F.A., Romein, J.W., 2018. Cobalt: A GPU-based correlator and beamformer for LOFAR. *Astronomy and Computing* 23, 180. 1801.04834.
- Corda, S., Veenboer, B., Awan, A.J., Romein, J.W., Jordans, R., Kumar, A., Boonstra, A.J., Corporaal, H., 2022. Reduced-precision acceleration of radio-astronomical imaging on reconfigurable hardware. *IEEE Access* 10, 22819–22843.
- Cucho-Padin, G., Wang, Y., Li, E., Waldrop, L., Tian, Z., Kamalabadi, F., Perillat, P., 2019. Radio frequency interference detection and mitigation using compressive statistical sensing. *Radio Science* 54, 986–1001. <https://agupubs.onlinelibrary.wiley.com/doi/pdf/10.1029/2019RS006902>.
- Fridman, P.A., Baan, W.A., 2001. RFI mitigation methods in radio astronomy. *Astronomy and Astrophysics* 378, 327–344.
- Gehlot, B.K., Koopmans, L.V.E., Brackenhoff, S.A., Ceccotti, E., Ghosh, S., Höfer, C., Mertens, F.G., Mevius, M., Munshi, S., Offringa, A.R., Pandey, V.N., Rowlinson, A., Shulevski, A., Wijers, R.A.M.J., Yatawatta, S., Zaroubi, S., 2024. Transient RFI environment of LOFAR-LBA at 72–75 MHz. Impact on ultra-widefield AARTFAAC Cosmic Explorer observations of the redshifted 21-cm signal. *Astronomy and Astrophysics* 681, A71. 2311.03023.
- Guo, C., Chen, S., Feng, C., Zeng, Z., 2015. Correlation-statistics-based spectrum sensing exploiting energy and polarization for dual-polarized cognitive radios. *IEEE Transactions on Wireless Communications* 14, 1533–1554.
- Guo, C., Wu, X., Feng, C., Zeng, Z., 2013. Spectrum sensing for cognitive radios based on directional statistics of polarization vectors. *IEEE Journal on Selected Areas in Communications* 31, 379–393.
- Haarvoja, T., Zhou, A., Abbeel, P., Levine, S., 2018a. Soft Actor-Critic: Off-Policy Maximum Entropy Deep Reinforcement Learning with a Stochastic Actor. *arXiv e-prints*, arXiv:1801.012901801.01290.
- Haarvoja, T., Zhou, A., Hartikainen, K., Tucker, G., Ha, S., Tan, J., Kumar, V., Zhu, H., Gupta, A., Abbeel, P., Levine, S., 2018b. Soft Actor-Critic Algorithms and Applications. *arXiv e-prints*, arXiv:1812.059051812.05905.
- Hellbourg, G., Weber, R., Capdessus, C., Boonstra, A.J., 2012. Cyclostationary approaches for spatial RFI mitigation in radio astronomy. *Comptes Rendus Physique* 13, 71–79. The next generation radiotelescopes / Les radiotélescopes du futur.
- Ho, N.M., Wong, W.F., 2017. Exploiting half precision arithmetic in Nvidia GPUs, in: 2017 IEEE High Performance Extreme Computing Conference (HPEC), pp. 1–7.
- Kazemi, S., Yatawatta, S., 2013. Robust radio interferometric calibration using the t-distribution. *Monthly Notices of the Royal Astronomical Society* 435, 597–605.
- Leshem, A., van der Veen, A.J., 2000. Introduction to Interference Mitigation Techniques in Radio Astronomy, in: Smolders, A.B., van Haarlem, M.P. (Eds.), *Perspectives on Radio Astronomy: Technologies for Large Antenna Arrays*, p. 201.
- Leshem, A., van der Veen, A.J., Boonstra, A.J., 2000. Multichannel interference mitigation techniques in radio astronomy. *The Astrophysical Journal Supplement Series* 131, 355–373.
- Luo, W., Fan, R., Li, Z., Du, D., Wang, Q., Chu, X., 2024. Benchmarking and dissecting the nvidia hopper gpu architecture, in: 2024 IEEE International Parallel and Distributed Processing Symposium (IPDPS), pp. 656–667.
- Nita, G.M., Gary, D.E., 2010. The generalized spectral kurtosis estimator. *Monthly Notices of the Royal Astronomical Society* 406, L60–L64. 1005.4371.
- Nita, G.M., Hellbourg, G., 2020. A cross-correlation based spectral kurtosis RFI detector, in: 2020 XXXIIIrd General Assembly and Scientific Symposium of the International Union of Radio Science, IEEE. pp. 1–4.
- Offringa, A., de Bruyn, A., Biehl, M., Zaroubi, S., Bernardi, G., Pandey, V., 2010. Post-correlation radio frequency interference classification methods. *Monthly Notices of the Royal Astronomical Society* 405, 155–167.
- Rafei-Ravandi, M., Smith, K.M., 2023. Mitigating Radio Frequency Interference in CHIME/FRB Real-time Intensity Data. *The Astrophysical Journal Supplement Series* 265, 62. 2206.07292.
- Raza, J., Boonstra, A.J., Van der Veen, A.J., 2002. Spatial filtering of RF interference in radio astronomy. *IEEE Signal Processing Letters* 9, 64–67.
- Sclocco, A., Vohl, D., Van Nieuwpoort, R.V., 2020. Real-Time RFI Mitigation for the Apertif Radio Transient System. *arXiv e-prints*, arXiv:2001.033892001.03389.
- Smith, E., 2022. Impact of Radio Frequency Interference and Real-Time Spectral Kurtosis Mitigation. Ph.D. thesis. West Virginia University, 11467.
- Smith, E., Lynch, R.S., Pisano, D.J., 2022. Simulating Spectral Kurtosis Mitigation against Realistic Radio Frequency Interference Signals. *Astronomical Journal* 164, 123. 2207.07642.
- Sokolowski, M., Wayth, R.B., Lewis, M., 2016. The statistics of low frequency radio interference at the Murchison Radio-astronomy Observatory. *ArXiv e-prints* 1610.04696.
- Sutton, R.S., Barto, A.G., 2018. Reinforcement Learning: An Introduction. A Bradford Book, Cambridge, MA, USA.
- Van Nieuwpoort, R., Van Leeuwen, J., Sclocco, A., Spreeuw, H., Williams, C., 2018. Real-time RFI mitigation for LOFAR, Apertif and SKA, Institute of Electrical and Electronics Engineers Inc.
- Van Nieuwpoort, R.V., 2016. Towards exascale real-time RFI mitigation, in: 2016 Radio Frequency Interference (RFI), pp. 69–74.
- Vos, E.E., Francois Luus, P.S., Finlay, C.J., Bassett, B.A., 2019. A generative machine learning approach to RFI mitigation for radio astronomy, in: 2019 IEEE 29th International Workshop on Machine Learning for Signal Processing (MLSP), pp. 1–6.
- Vruno, F.D., Winkel, B., Bassa, C.G., Jozsa, G.I.G., Brentjens, M.A., Jessner, A., Garrington, S., 2023. Unintended electromagnetic radiation from starlink satellites detected with LOFAR between 110 and 188 MHz. *Astronomy and Astrophysics* 1, arXiv:2307.02316. <https://doi.org/10.1051/0004-6361/202346374>.
- van Werkhoven, B., 2019. Kernel tuner: A search-optimizing GPU code auto-tuner. *Future Generation Computer Systems* 90, 347–358.
- Winkel, B., Jessner, A., 2019. Compatibility between wind turbines and the radio astronomy service. *Journal of Astronomical Instrumentation* 08, 1940002. <https://doi.org/10.1142/S2251171719400026>.
- Yatawatta, S., 2021. Polarization-based online interference mitigation in radio interferometry, in: 2020 28th European Signal Processing Conference (EUSIPCO), pp. 1961–1965.

Yatawatta, S., 2024. Reinforcement learning. *Astronomy and Computing* 48, 100833.